



ELSEVIER

Contents lists available at ScienceDirect

## Journal of Magnetism and Magnetic Materials

journal homepage: [www.elsevier.com/locate/jmmm](http://www.elsevier.com/locate/jmmm)Grain size and interfacial interdiffusion influence on the magnetic and dielectric properties of magnetoelectric  $\text{La}_{0.7}\text{Ba}_{0.3}\text{MnO}_3\text{-BaTiO}_3$  compositesJ.L. Clabel H.<sup>a,\*</sup>, F.A. Ferri<sup>b</sup>, F.L. Zabotto<sup>b</sup>, V.A.G. Rivera<sup>c</sup>, I.C. Nogueira<sup>d</sup>, D. Garcia<sup>b</sup>, O.F. de Lima<sup>e</sup>, E.R. Leite<sup>f</sup>, M.A. Pereira-da-Silva<sup>a,g</sup>, C.A. Cardoso<sup>b</sup><sup>a</sup> Institute of Physics of São Carlos, University of São Paulo, São Carlos, SP, Brazil<sup>b</sup> Department of Physics, Federal University of São Carlos, São Carlos, SP, Brazil<sup>c</sup> Escuela de Física, Universidad Nacional Federico Villarreal, Lima, Lima, Perú<sup>d</sup> Instituto Federal do Maranhão, PPG em Engenharia de Materiais, São Luís, MA, Brazil<sup>e</sup> Institute of Physics "Gleb Wataghin", University of Campinas, Campinas, SP, Brazil<sup>f</sup> Department of Chemistry, Federal University of São Carlos, São Carlos, SP, Brazil<sup>g</sup> Paulista Central University Center, UNICEP, Sao Carlos, SP, Brazil

## ARTICLE INFO

## Article history:

Received 2 January 2016

Received in revised form

18 January 2016

Accepted 25 January 2016

Available online 26 January 2016

## Keywords:

Dielectric properties

Magnetic properties

Laminated composite

Magnetoelectric coupling

## ABSTRACT

We report on specific features of the dielectric and magnetic properties as well as magnetoelectric coupling coefficients ( $\alpha^{ME}$ ) of the  $\text{La}_{0.7}\text{Ba}_{0.3}\text{MnO}_3$  (L)- $\text{BaTiO}_3$  (B) 2–2 type ceramic composite. The powder of L and B was synthesized by two different methods (solid state reaction and Pechini). Orthorhombic and tetragonal phases were observed for the separated phases L and B of the composite, respectively, for both synthesis methods. The characteristics of grain size and interfacial interdiffusion in the L–B–L composite obtained for different synthesis method were studied, showing that diffusion was a typically physical migration, which can be mainly controlled by the grain size. Anomalies in the observed dielectric behavior are attributed to the internal residual stresses and chemically inhomogeneous regions. The existence of a broad magnetic transition observed in the pure L phase and laminated L–B–L composite was also attributed to its small grain size. A comparison of the maximum transversal ( $\alpha_{31}^{ME}$ ) and longitudinal ( $\alpha_{33}^{ME}$ ) ME coupling coefficients, at room temperature, is also shown.

© 2016 Elsevier B.V. All rights reserved.

## 1. Introduction

The magnetoelectric (ME) effect has attracted great interest in the field of multiferroic materials, due to the possible control of the magnetic (ferroelectric) order via an applied electric (magnetic) field [1–3], which has enormous implications from the technological point of view [4–6]. A great deal of effort has been dedicated to investigating multiferroic composites due to the ME response, exploring all different connectivity schemes possible for bulk samples (e.g. 0–3 type particulate composite, 2–2 type laminate composite and 1–3 type rod composite) [7–15]. ME effect shows to be several orders of magnitude larger in multiferroic composites than in single-phase multiferroic [7–9]. 2–2 type multiferroic composite has been shown to present superior properties than other connectivity schemes due to the reduced problems with diffusion/reaction between its phases. Therefore, it

has drawn considerable interest for the fabrication of magnetoelectric devices [10–13]. Several different materials have been tried as piezoelectric or magnetic phase in those compound, as Terfenol-D/PZT [7], LCMO/PZT [11] and NCZF-(0.9 PZT-0.1 PZN)-NCZF [9], including single phase compounds such as  $\text{La}_{0.1}\text{Bi}_{0.9}\text{MnO}_3$  [16] with ferromagnetic and ferroelectric properties. The  $\text{La}_{0.7}\text{Ba}_{0.3}\text{MnO}_3$  (L) manganite with perovskite structure exhibits a ferromagnetic transition temperature as high as  $T_C \approx 310$  K [17]. The manganite have been the subject of intense investigations due to their colossal magnetoresistance (CMR) and giant volume magnetostriction [17–20]. On the other hand, barium titanate is one of the most widely studied ferroelectric due to its good dielectric and piezoelectric properties [21,22]. Therefore, L and B are promising candidates because of their giant magnetostriction (L phase) and high dielectric constant (B phase) in room temperature to obtain a strong ME effect. Furthermore, dielectric, magnetic and ME properties of these 2–2 type composites have not yet been systemically investigated.

Therefore, we report 2–2 type ME composite consisting of a B layer (piezoelectric material) sandwiched by L layers on top and

\* Corresponding author.

E-mail address: [jclabel@ifsc.usp.br](mailto:jclabel@ifsc.usp.br) (J.L. Clabel H.).

bottom (magnetostrictive/ferromagnetic materials), i.e., L–B–L, as an attractive candidate for 2–2 type composite, due to their dielectric, magnetic and ME properties at room temperature. The dielectric, magnetic and ME properties of the L–B–L composite samples are investigated and discussed in correlation with their structural and microstructural features.

## 2. Experimental

Powders of the pure phases of the L–B–L 2–2 type composites, B and L, were prepared employing the solid-state reaction (SSR) and Pechini (P) method. For SSR method,  $\text{BaCO}_3$  (99.9%),  $\text{TiO}_2$  (99%), and  $\text{BaCO}_3$  (99.9%),  $\text{MnCO}_3$  (99.9%),  $\text{La}_2(\text{CO}_3)_3$  (99.9%) powders were weighed according to the desired stoichiometric composition B and L, respectively. B and L, separately, were mixed in a ball mill using isopropyl alcohol as solvent and zirconium oxide balls as the milling medium, for 24 h. Then, they were dried and calcinated at 1000 °C for 2 h (B) and 1200 °C for 1 h (L) in an alumina crucible. The precursor powders were mixed separately, using a mortar and pestle, for 0.3 h in a solvent (distilled water), at a ratio of 1 g of precursor to 50  $\mu\text{l}$   $\text{H}_2\text{O}$ , so as to facilitate the conformation process. The detailed procedure of the synthesized powders from P method to B and L is reported elsewhere [23].

The single-phase (L and B) and the L–B–L 2–2 type composites were subsequently sintered at a temperature of 1200 °C for 2 h. The L–B–L laminated ceramic composite was fabricated by means of mechanical coupling between the two phases, without epoxy resin for their junction. The final laminated composite of cylindrical geometry with 8 mm diameter and 1.2 mm thickness, was formed by pressing at 140 MPa and sintering at 1200 °C for 2 h. The single-phase samples and the L–B–L composites were polished and electrical contacts were made with Ag paste on both sides. The laminated composites were then polarized in an oil bath under a DC field of 2 kV/mm for 30 min at room temperature. The X-ray diffraction (XRD) patterns of the single-phase and the L–B–L composites were taken using a DMax-2500PC diffractometer (Rigaku) with  $\text{Cu-K}\alpha$  radiation ( $\lambda = 1.5406 \text{ \AA}$ ), at room temperature, with the  $2\theta$  ranging from 10° to 110° with a step size of  $0.02^\circ \text{ min}^{-1}$ . Rietveld refinement of the XRD data was carried out using the general structure analysis program (GSAS) [24]. The morphologies of the surfaces are investigated by means of a FEG-EDX instrument (Model XL-30, Philips) operated at 25 kV. The real and imaginary parts of dielectric permittivity,  $\epsilon'$  and  $\epsilon''$  respectively, were measured under 0.1 to 10,000 kHz frequency using an HP 4194A precision LCR meter. Magnetic properties were measured in the 50–350 K range employing a Vibrating Sample Magnetometer (VSM). The ME measurement were carried out using the lock-in technique [25]. The response was measured in terms of the variation of the ME coefficient as a function of the applied DC magnetic field up to 10 kOe.

## 3. Results and discussion

Fig. 1 shows the evolution of the lattice parameters and cell volume with grain size, for the pure L and B phases of the L–B–L 2–2 type composite, synthesized from SSR and P methods. For both synthesis methods, the structure refinement data confirmed a tetragonal symmetry (B layers) with space group  $\text{P4}/\text{mm}$  according to the standard ICSD (Inorganic Crystal Structure Database) N° 67520 [26], and a rhombohedral symmetry (L layers) with space group  $\text{R-3cH}$  according to the standard ICSD N° 94815 [27]. It is not observed considerable changes in the cell parameter as well as in the cell volume in the pure L phase. However, with the increase of the grain size it shows an increasing in cell volume. From the

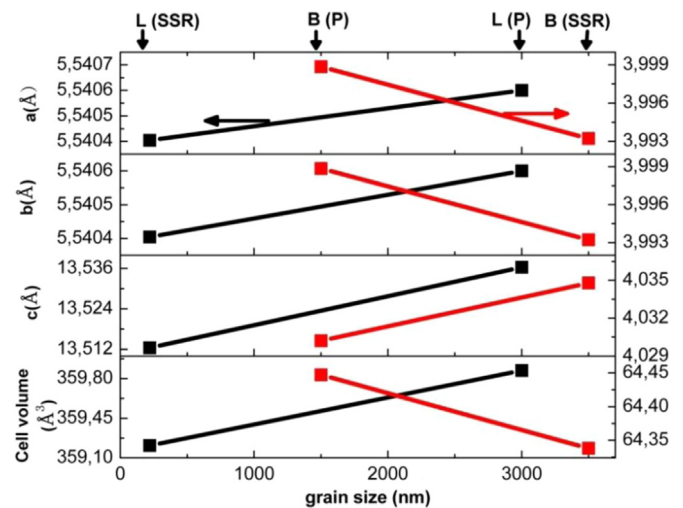


Fig. 1. Variation of the red parameter a, b, c and unit cell volume with grain size at 300 K for the pure L phase and pure B phase synthesized with solid-state reaction (SSR) and Pechini (P) methods. (For interpretation of the references to color in this figure legend, the reader is referred to the web version of this article.)

Rietveld refinement the average tetragonality ( $c/a$ ) for the pure B phase of the L–B–L 2–2 type composite synthesized for SSR method was  $c/a \approx 1.011$ , showing relatively higher tetragonality in comparison with  $c/a \approx 1.007$  for the pure B phase of the L–B–L 2–2 type composite synthesized for P method. This result is slightly higher than the reported structural data by T. Sundararajan et al. [28], for B obtained by SSR method, with grain size of 0.12  $\mu\text{m}$ .

The scanning electron microscopy (SEM) images of grain size distribution of the L–B–L composite are shown in Fig. 2(a), for the SSR method. The microstructure of the fractured composite sintered for 2 hours in 1200 °C indicates the formation of a well-defined interface, with grain average sizes of  $\sim 0.35 \mu\text{m}$  and  $\sim 0.30 \mu\text{m}$  for B and L layers, respectively, as observed in the inset of Fig. 2(a). In addition, the presence of porosity is observed in accordance to the relative density of the  $\sim 90\%$  obtained in these composite systems. In fact, as reported earlier based on the same compositions of laminate composite for the P method [23], where the average grain size was  $\sim 0.5 \mu\text{m}$  and  $\sim 2 \mu\text{m}$  for the B and L layer, respectively, with similar relative density. Both synthesis methods will result in a different crystallite growth, particle size and agglomeration. All these changes will affect the sintering behavior of the materials. Especially, during the thermal treatment of the laminated composites leading to dissimilar microstructural features, where different reactions take place for both methods and produce different behaviors.

The chemical composition of the L and B layers is shown in the Fig. 2(b), for the SSR (top) and Pechini (lower) method. Here, energy dispersive X-ray spectroscopy (EDS) spectra were realized. The element distribution, for the SSR method, taken along the horizontal line indicates the average boundary location as shown in the Fig. 2(a). The elemental composition ratio of the L and B layers were confirmed, indicating that L and B layers were preserved across the interface without any secondary reaction. For SSR method Fig. 2(b) top, the upright line indicates the boundary location where the element concentrations falls abruptly when there are changes from L layers (B layers) to B layers (L layers), demonstrating that there is negligible interdiffusion when sintered at 1200 °C, compared with other studies on 0–3 and 2–2 type composites [23,29]. On the other hand, for the Pechini method Fig. 2(b) bottom, the element concentration decrease gradually with progress of the transition from L layers (B layers) to B layers (L layers). Two possible causes are described for low Ba in relations

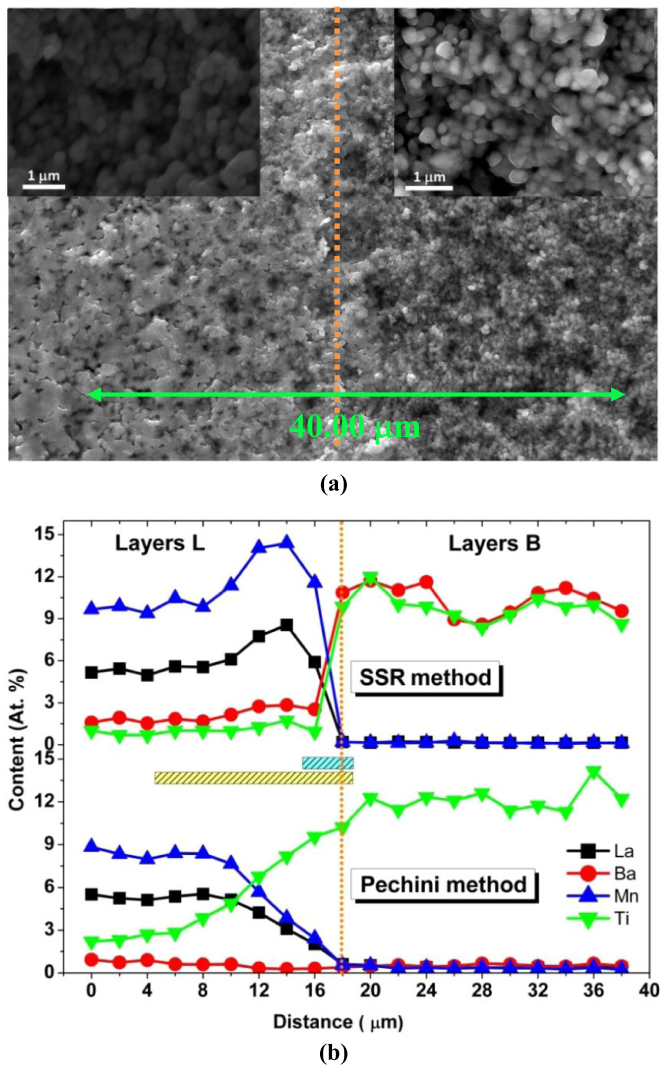


Fig. 2. (a) Cross-sectional SEM image of B layers (right) and L layers (left) (b) Distribution of elements across the boundary. The vertical dotted line indicates the average boundary. The inset in (a) represents the grain size of the B and L layers.

to Ti concentration in the B layers: a) substitution of Ba ions by La ions or excess Ti could lead to Ba deficiency [23]. b) Considering that the energy resolution of EDS imposes a limit on the separation of peak, the peak overlap between lines of same shells and different shells commonly occur. However, the identification of peaks is generally not a problem, but overlapping peaks require deconvolution and it is not always possible to separate properly these peaks. In this sense, the  $L_{\alpha}$  emission line of element of Ba overlaps with the  $K_{\alpha}$  emission line of Ti, this may be a consequence of absence of Ba. Thus, the Fig. 2(b) must be examined in a carefully and qualitative way. The dashed bars indicated the interdiffusion between the B and L layers to both methods. We note that the dashed bars for SSR method ( $\sim 4 \mu\text{m}$ ) are much smaller than the dashed bars for Pechini method ( $\sim 17 \mu\text{m}$ ). The variation in the interdiffusion mechanism in the interface of the L–B–L composite synthesized with SSR and P methods can be explain as follow: the driving force for the sintering process is the decrease of surface Gibbs energy which occurs as the surface area of the grain is reduced [30]. Simultaneously, the grains will grow in order to decrease the interfacial Gibbs energy of the grain boundary. In the sintering process of micron-sized precursor powders the surface diffusion is only responsible for particle coarsening during the initial stage of sintering but is not influential in the densification

[31]. Grain boundary diffusion is activated at higher temperatures than surface diffusion and also contributes to grain growth which is observed in the final stage of sintering. When nanometer sized precursor powders are used the contribution of surface diffusion to the densification process cannot be ignored because it implies the presence of large surface areas that in turn affect the development of the particle/pore structure during sintering. The grain growth takes place in the final stage of the sintering of micron-sized powders. However, in the case of nanometer sized powders it seems that grain growth occurs simultaneously with the densification from the very beginning of the sintering process. Considering the particles size of precursor powders of the pure phases for P method (L $\sim 150$  nm and B $\sim 250$  nm) and SSR method (L $\sim 200$  nm and B $\sim 260$  nm), the grain growth takes place simultaneously with densification, i.e., happens both a surface diffusion and a grain boundary diffusion inducing. After the sintering process, the Gibbs energy of small grain sizes (SSR method) is larger than that of large grain sizes (P method). However, the grain boundary diffusion in large grain sizes is higher in large grains, i.e., the interdiffusion can be induced progressively according to grain size, as shown in the Fig. 2(b).

The real ( $\epsilon'$ ) and imaginary ( $\epsilon''$ ) parts of electric permittivity as a function of temperature and frequency for the pure B phase and laminate L–B–L composite synthesized for SSR method is shown in Fig. 3(a–b). The values of the real part of electric permittivity at room temperature ( $\epsilon_{rt}'$ ) and maximum value ( $\epsilon_{max}'$ ) dielectric loss ( $\tan \delta$ ) and the temperature which  $\epsilon'$  is maximum ( $T_m$ ), are Table 1 summarized, for the B phase and laminate L–B–L composite. It can be seen in the Fig. 3 and in the Table 1 that the dielectric properties shows maximum values close to 400 K. For B system Fig. 3 (a), the polarization vanishes for temperatures higher than 400 K accompanied to the maximization of dielectric constant, which is associated to the ferroelectric–paraelectric structural phase transitions. Thus, the  $T_m$  values observed for the studied materials are related to this ferroelectric–paraelectric phase transition in the B matrix. However, it can be seen a shift of  $T_m$  temperature from 400 K to 445 K for laminate L–B–L composite obtained from SSR method Fig. 3(b), compared to the laminated for P method. Generally, shifts in the  $T_m$  are occasioned by the residual stress in the ferroelectric phase or chemically changes of stoichiometry. Since the XRD pattern shows a concordance to the expected to B structure, the shift for high temperature may be consequence of the internal residual stresses in the laminate L–B–L composite when cooled from a high temperature to below  $T_m$  due to different shrinkage between phases or generated by decrease of grain size, in agreement to the reported by R.C. Rice et al. [32] In addition, it can be seen, from the Table 1, that the electric permittivity values  $\epsilon_{rt}'$  and  $\epsilon_{max}'$  is dependent of the synthesis method. To P method, the  $\epsilon'$  value for pure B phase is lower than that laminate L–B–L composite. Analogously, to SSR method the  $\epsilon'$  value is strongly depressed in comparison to P method. The values of electric permittivity is strongly dependent mainly for grain size and internal stress of structure [32, 33]. The samples sintered by the P method, it is observed a decrease of grain size in the B phase compared with its composite, which result in lower electric permittivity values. Similar results is observed comparing composites from P and SSR method, which lower electric permittivity values is accompanied by a reduction of grain size for SSR method. The grain size dependence of the permittivity observed in this study, from of both methods, is in good agreement with the results reported in the literature [33–35].

The  $\epsilon'$  and dielectric losses tangent ( $\tan \delta$ ) value as a function of frequency of the pure B phase and laminate L–B–L composite is presented in Fig. 3(c–d). For pure B phase by P method, the frequency dependence of  $\epsilon'$  in room temperature shown  $\epsilon'$  decreases rapidly up to  $10^5$  Hz and beyond has a slow fall, Fig. 3(c).

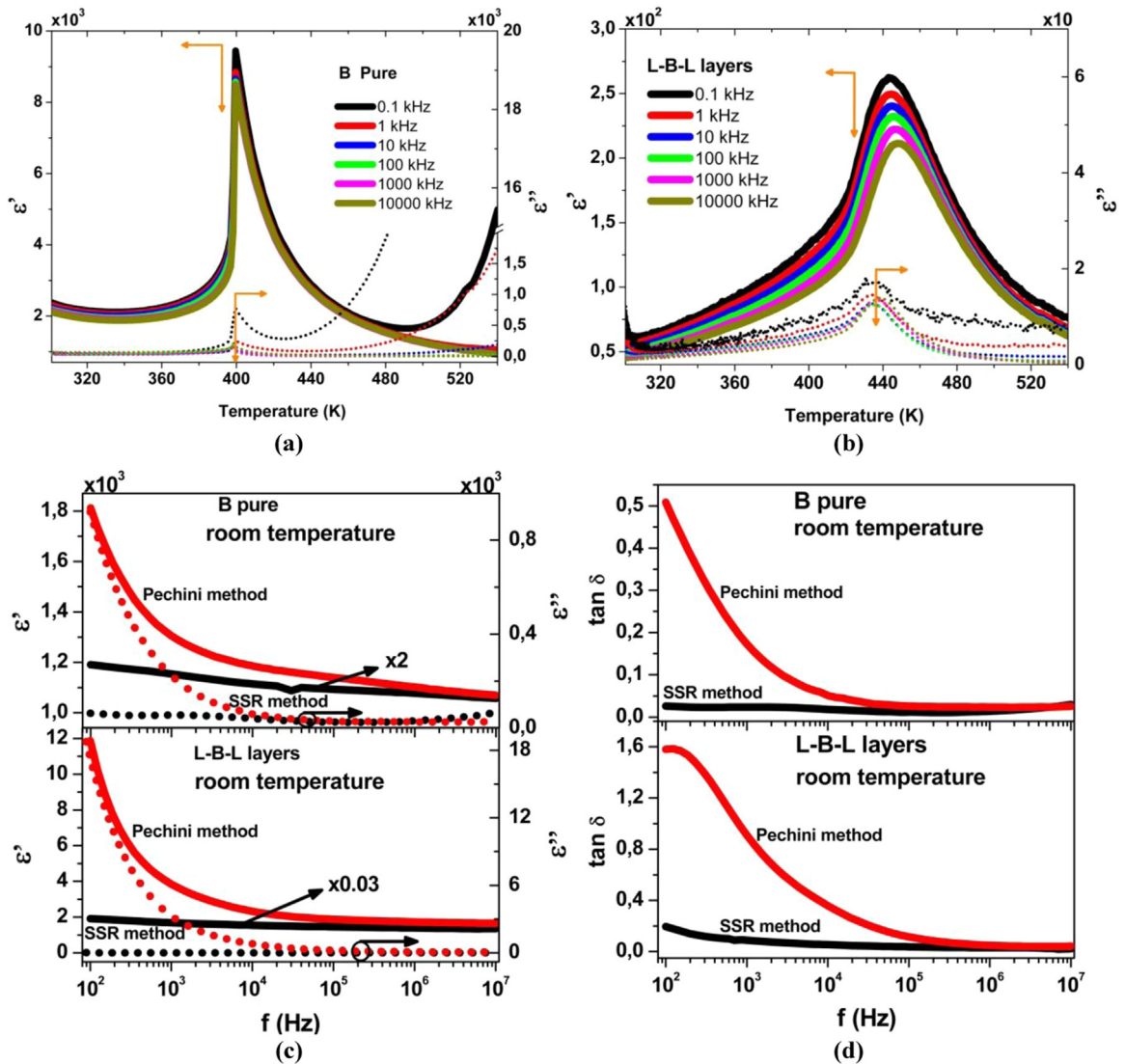


**Fig. 3.** (a–b) Temperature dependent dielectric spectra  $\epsilon'$  and  $\epsilon''$  of the pure B phase and L–B–L layers, respectively, for SSR method. (c–d) frequency dependence of dielectric constant at various temperature, of the pure B phase and L–B–L layers, respectively, for SSR and P method.

**Table 1**

The temperature of dielectric constant maximum ( $T_{max}$ ), dielectric constant in room temperature  $\epsilon_{rt}'$  and maximum  $\epsilon_{max}'$ , and dielectric loss ( $\tan \delta$ ) for the samples at 1 kHz.

Sample	Method	$\epsilon_{rt}'$	$\epsilon_{max}'$	$T_m$ (K)	$\tan \delta (T_{room})$
B	SSR	2200	8840	400	0.02
B*	P	1295	1561	403	0.17
L–B–L	SSR	57	249	445	0.08
L–B–L*	P	3690	2970	402	0.90

Values from of the reference [23].

Analogously, by SSR method the  $\epsilon'(f)$  is higher than that P method, notwithstanding has a slow fall over the frequency. Already in laminate L–B–L composites  $\epsilon'(f)$  response is otherwise observed in pure B phase. This behavior is attributed to the combination of grain size density and interfacial polarization due to extrinsic contributions as the presence of point defect product of synthesis method. In frequency  $> 10^5$  Hz is observed the process relaxation of the interfacial polarization. The dielectric losses at room temperatures, as shown Fig. 3(d), of the samples from of the P method follow the same trend, decreases rapidly with frequency increasing and then reaches a constant value. On the other hand, it is

interesting to note that by SSR method, the dielectric losses are independent of frequency at lower frequencies below  $10^5$  Hz. Considered Maxwell–Wagner effect [36], in low frequency this is associated to the thermally activated space charge effect which is negligible and high conductivity of L phase [17], in low frequency, in samples by the SSR method.

Magnetization ( $M$ ) versus temperature ( $T$ ) profile of the pure L sample and laminate L–B–L composite for SSR method was measured in a DC applied field of 50 Oe, as shown Fig. 4(a). The Curie temperatures  $T_C$  (defined as the corresponding peak of  $\frac{dM}{dT}$  from the  $M$  versus  $T$  curves) are 334 K and 332 K for the pure L phase and laminated L–B–L composite, respectively. Manh-Huong Phan et al. [37] and Asish K. Kunduet et al. [38] report values of  $T_C$  slightly higher than our result, for pure L phase. A comparison of the pure L phase and laminated L–B–L composite regarding the magnetic behavior shows that they differ slightly in the magnitude of the magnetization maximum with values of 4.3 and 3.9  $\text{emu g}^{-1}$  when  $T < T_C$ , but with a similar broad magnetic transition. The slight decrease in magnetization and the shift to lower temperatures of  $\frac{dM}{dT}$  in laminated L–B–L composite can be attributed to the presence of a nonmagnetic layer (B layer) due to two factors: (i) B layer can induce a decreasing in the particle size in the L layers due

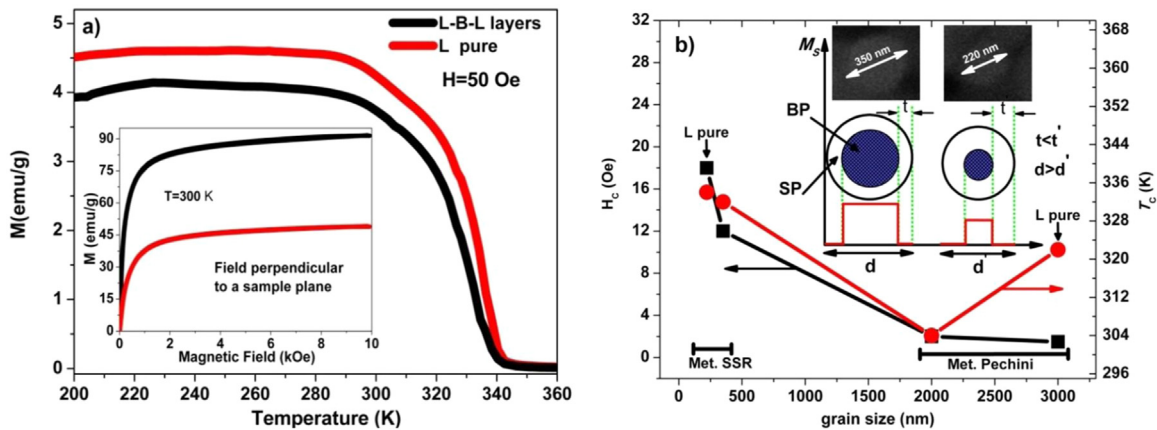


**Fig. 4.** (a) Magnetization as a function of temperature for L pure sample (red) and laminate L–B–L composite (black), for SSR method (b) Variation of the coercive field ( $H_C$ ) and  $T_C$  as a function of the average grain diameter ( $d$  and  $d'$ ). The inset in (a) is the Magnetization versus field at  $T=300$  K for pure L sample and laminate L–B–L composite for SSR method. The inset in (b) is a schematic representation of the body phase (BP) and surface phase (SP) for the grains. (For interpretation of the references to color in this figure legend, the reader is referred to the web version of this article.)

to the differences in thermal expansion during the sintering process of the laminated L–B–L composite. (ii) The contribution of the diamagnetic regions (B layer) [39] in the interphase on the total magnetization is somewhat lesser than in the L layers. In this context, Kameli, P. et al. [40] and F. Millange et al. [41] reported a shift of the phase transition to high temperatures, without a broad phase transition with the increase of grain size. They explain this behavior in terms of grain boundary effects and due to  $\text{La}^{3+}$  and  $\text{Ba}^{2+}$  cations ordering, respectively. An explanation for the broad magnetic transition has been proposed for granular perovskite system with nanometer grain size which considered that the system can be divided in a body phase and a surface phase ( $t$ ), Fig. 1 [42,43]. Body phase would have the same properties as the bulk compound (oxygen stoichiometry, magnetic and transport properties). The break of the  $\text{Mn}^{3+}-\text{O}^{2-}-\text{Mn}^{4+}$  bonds of the magnetic phase can induce localization of the  $e_g$  electrons (from  $\text{Mn}^{3+}$  ions) both in the surface phase of the pure L sample and L layers of the laminated L–B–L composite. Consequently, the double exchange interaction in the samples is weakened, in which the electron spins form disordered ferromagnetic alignment of the constituent manganese ions. Therefore, the broadened transition observed here is due to the magnetic disorder in the surface phase of the grains, since that surface phase is increased with the decrease of the grain size. Likewise, magnetization magnitude and transition temperature in laminated L–B–L composite and pure L sample is almost similar, and indicated that the body-surface contribution to the magnetization is nearly the same. This subtle difference suggests that the grain surface phase expands with the presence of the non-magnetic layers accompanied of defect chemical of the laminated L–B–L composite, mentioned above. Meanwhile, the magnetism is weakened in the laminated L–B–L composite and the range of the magnetic transition is broadened. In consequence, there is a smaller contribution of the B layer (non-magnetic) in the total magnetization than in the L layers.

The room temperature magnetization as a function of applied magnetic field up to 10 kOe was measured using a VSM for L pure sample and laminate L–B–L composite, inset of Fig. 4(a). All the samples show ferromagnetic nature, with lower values of coercive field (soft ferromagnetic). The coercive field ( $H_C$ ) is equal to 12 and 18 Oe for the L pure sample and laminate L–B–L composite after sintering at 1200 °C, respectively. This is in agreement whereas that the grain size in the L layer of the laminate L–B–L composite is larger than in the pure L sample. Trukhanov, S. V. et al. [44] reported a similar coercive field for a grain size 200 nm lower, with a value lower than 16 Oe. The saturation magnetization in the

laminated L–B–L composite ( $\sim 84.4 \text{ emu g}^{-1}$ ) is higher than in pure L sample ( $\sim 43.9 \text{ emu g}^{-1}$ ), as shown in Fig. 4(a). In (b), we show the comparison of the evolution of the  $H_C$  and  $T_C$  as a function of grain size for the samples fabricated with the SSR method and Pechini method [23]. The inset of Fig. 4(b) shows a general phenomenological demonstration of the magnetic order/disorder in the body phase (BP) and surface phase (SP) of the nanometric grains. The body phase has diameters ( $d - 2t$ ) and ( $d' - 2t'$ ), where  $t$  and  $t'$  are the thickness of the surface phase, which is dependent of the grain size. The difference on saturation magnetization and coercive field with the reduction in grain size as observed is attributable to the presence of a non-magnetic dead layer on the surface phase created by non-crystalline material that is more significant as the grain size decreases. The larger surface phase lead to a decrease in the saturation magnetization with the decrease in grain size. Thus,  $H_C$  tends to grow due to the larger surface phase accompanied by the grain size decreasing. The grain size is in agreement with the SEM-FEG images of the fractured surface shown in Fig. 2(a).

In order to demonstrate the coupling between electric and magnetic order in laminated L–B–L composite, the magneto-electric coupling coefficient was measured under longitudinal ( $\alpha_{33}^{ME}$ ) and transverse ( $\alpha_{31}^{ME}$ ) conditions, for composites grown by both SSR and P methods. The measurements were, performed at ac magnetic field of 1 kHz and they are presented in Fig. 5(a–b). The  $\alpha_{31}^{ME}$  and  $\alpha_{33}^{ME}$  values, for laminate L–B–L composite for SSR method, increase sharply to the maximum value of about 0.65 and 0.26  $\text{mV cm}^{-1} \text{Oe}^{-1}$  at 0.04 kOe and 2 kOe magnetic field, respectively, Fig. 5(a). For laminate L–B–L composite for P method, Fig. 5(b) shows a similar behavior with  $\alpha_{31}^{ME}$  and  $\alpha_{33}^{ME}$  values 0.55 and 0.52  $\text{mV cm}^{-1} \text{Oe}^{-1}$  at 0.31 kOe and 2.93 kOe magnetic field, respectively. For both methods, the answer  $\alpha_{31}^{ME}$  maximum is very low with applied magnetic field being eight times lower for the SSR method than P method. On the other hand,  $\alpha_{31}^{ME}$  (SSR method) features a narrow peak and a quick drop to negative values than to  $\alpha_{31}^{ME}$  (P method), with dependence of applied magnetic field. The values for  $\alpha_{31}^{ME}$  are slight higher that reported for the same laminate L–B–L composite [23], but lower than reported by Srinivasan et al. [11,15]. Such changes in the magnetoelectric coefficient can be associated to the grain size, inter-diffused layer between phases and porosity mainly in the piezoelectric phase, as observed in the microscopy of samples. Since the ME coefficient is due to mechanical coupling between two distinct phases, porosity and inter-diffused layer diminishes the mechanic coupling decreasing the conversion of strain generated by magnetic field in the strain on

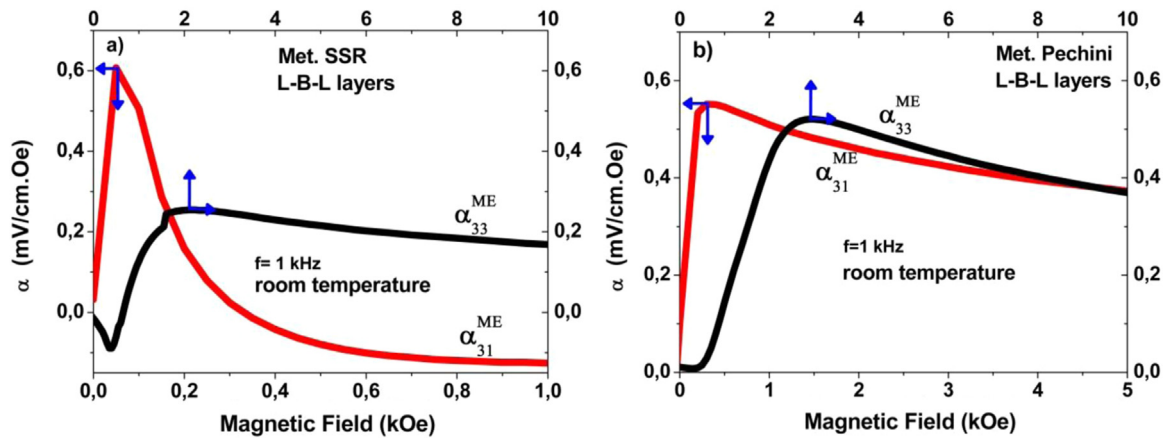


**Fig. 5.** ME coefficient curve dependence on magnetic field for the laminated L–B–L composite measured at 300 K and 1 kHz, showing the longitudinal ( $\alpha_{33}^{ME}$ ) and transverse ( $\alpha_{31}^{ME}$ ) ME coefficients vs H for laminate composite for SSR (a) and P (b) method.

the piezoelectric phases. Added to these extrinsic effects, the reduction of piezoelectric grain size diminishes the piezoelectric properties due to increase of internal stress, which also affect the ME voltage conversion. Two facts distinguishable are observed from the Fig. 5: (i) The maximum value of  $\alpha_{31}^{ME}$  is achieved for very low applied field (lower two order of magnitude in comparison of  $\alpha_{33}^{ME}$ ) lower than those reported by Srinivasan et al. [11,15] for a bilayer of  $\text{La}_{0.7}\text{Sr}_{0.3}\text{MnO}_3/\text{PZT}$ , and, (ii) The difference of the maximum peak between  $\alpha_{31}^{ME}$  and  $\alpha_{33}^{ME}$  is originates from the influence of shape demagnetization on the magnetostriction of the magnetostrictive phase [15]. The strain of the L layers will induce stress in the B layer and then this generates charge carriers in the interface. Furthermore, with increase in DC field, the torque on magnetic dipoles unsettle maximum displacement of charge carriers, therefore, the voltage induced exhibits a maximum value, which decreases with increase in applied magnetic field.

#### 4. Conclusion

In summary,  $\text{BaTiO}_3$  (B),  $\text{La}_{0.7}\text{Ba}_{0.3}\text{MnO}_3$  (L) and laminate L–B–L composites are prepared employing the SSR and P method. Rietveld refinement shows that the rhombohedral to tetragonal phase of the L and B pure phase without any intermediate phase for both syntheses method. Analysis of the scanning electron microscopy reveals ideal interface conditions for the laminate L–B–L composite for SSR method. The anomalies between the pure B phase and laminate L–B–L composite for SSR method around  $\sim 43$  K is due to residual stresses due to the grain size effects and chemically inhomogeneous regions in the grain boundary. The saturation magnetization values for laminate L–B–L composite and pure L sample as well as coercive field are dependent of the grain size accompanied by the surface phase, for both methods. The variation in the magnetic phase transitions with variation in mole ratio of the constituent phase reflects the interactions between electric and magnetic dipoles of constituent phases on microscopic scale, though macroscopically the composite is a homogeneous structure. Although  $\alpha_{31}^{ME}$  at room temperature is small, i.e.,  $0.65 \text{ mV cm}^{-1} \text{ Oe}^{-1}$  for SSR method, we observe ME coupling maximum in a very low applied field, about 0.04 kOe. The variation of the behavior of  $\alpha_{31}^{ME}$  and  $\alpha_{33}^{ME}$  is due to the shape demagnetization. The same is higher for the sample prepared by P method. The grain size effect, due to synthesis method, of the L and B layer as well as the low density caused by differences in thermal expansion is responsible for the reduced ME coupling.

#### References

- [1] T. Kimura, T. Goto, H. Shintani, K. Ishizaka, T. Arima, Y. Tokura, Magnetic control of ferroelectric polarization, *Nature* 426 (2003) 55–58.
- [2] J.L. M.F. Thomas Lottermoser, Thomas Lonkai, Uwe Amann, Dietmar Hohlwein, Magnetic phase control by an electric field, *Nature* 430 (2004) 539–541.
- [3] M. Fiebig, Revival of the magnetoelectric effect, *J. Phys. D Appl. Phys.* 38 (2005) 123.
- [4] J. Ma, J. Hu, Z. Li, C.-W. Nan, Recent progress in multiferroic magnetoelectric composites: from bulk to thin films, *Adv. Mater.* 23 (2011) 1062–1087.
- [5] W. Eerenstein, N.D. Mathur, J.F. Scott, Multiferroic and magnetoelectric materials, *Nature* 442 (2006) 759–765.
- [6] R. Myers, R.A. Islam, M. Karmarkar, S. Priya, Magnetoelectric laminate composite based tachometer for harsh environment applications, *Appl. Phys. Lett.* 91 (2007) 122904.
- [7] K.U. H.-E.K. Jungho Ryu, Shashank Priya, Magnetoelectric effect in composites of magnetostrictive and piezoelectric materials, *J. Electroceram.* 8 (2002) 107–119.
- [8] S. Priya, R. Islam, S. Dong, D. Viehland, Recent advancements in magnetoelectric particulate and laminate composites, *J. Electroceram.* 19 (2007) 149–166.
- [9] R. a Islam, Y. Ni, A.G. Khachatryan, S. Priya, Giant magnetoelectric effect in sintered multilayered composite structures, *J. Appl. Phys.* 104 (2008) 044103.
- [10] J. Ryu, A.V. Azquez, K. Uchino, H. Kim, Piezoelectric and magnetoelectric properties of lead zirconate titanate/Ni-ferrite particulate composites, *J. Electroceram.* 7 (2001) 17–24.
- [11] G. Srinivasan, E. Rasmussen, B. Levin, R. Hayes, Magnetoelectric effects in bilayers and multilayers of magnetostrictive and piezoelectric perovskite oxides, *Phys. Rev. B* 65 (2002) 134402.
- [12] S.P., J.R. Kenji Uchino, Alfredo Vasquez Carazo, Effect of the magnetostrictive layer on magnetoelectric properties in lead zirconate titanate/terfenol-D laminate composites, *J. Am. Ceram. Soc.* 908 (2001) 2905–2908.
- [13] S. Dong, J.F. Li, D. Viehland, Giant magnetoelectric effect in laminate composites, *Philos. Mag. Lett.* 83 (2003) 769–773.
- [14] M.I. Bichurin, V.M. Petrov, G. Srinivasan, Theory of low-frequency magnetoelectric effects in ferromagnetic-ferroelectric layered composites, *J. Appl. Phys.* 92 (2002) 7681.
- [15] G. Srinivasan, Magnetoelectric composites, *Annu. Rev. Mater. Res.* 40 (2010) 153–178.
- [16] M. Gajek, M. Bibes, S. Fusil, K. Bouzehouane, J. Fontcuberta, A. Barthelemy, et al., Tunnel junctions with multiferroic barriers, *Nat. Mater.* 6 (2007) 296–302.
- [17] E. Dagotto, Springer Series in Solid-State Sciences: Nanoscale Phase Separation and Colossal Magnetoresistance, Ed. 1, New York, 2002.
- [18] R.V. Demin, L.I. Koroleva, Y.M. Mukovskii, Giant volume magnetostriction and colossal magnetoresistance at room temperature in  $\text{La}_{0.7}\text{Ba}_{0.3}\text{MnO}_3$ , *J. Phys. Condens. Matter* 17 (2005) 221–226.
- [19] C. Zener, Interaction between the D-shells in the transition metals. II. Ferromagnetic compounds of manganese with perovskite structure, *Phys. Rev.* 82 (1951) 403–405.
- [20] R.V. Demin, L.I. Koroleva, a Z. Muminov, Y.M. Mukovskii, Giant volume magnetostriction and colossal magnetoresistance in  $\text{La}_{0.7}\text{Ba}_{0.3}\text{MnO}_3$  at room temperature, *Phys. Solid State* 48 (2006) 322–325.
- [21] S. Shao, J. Zhang, Z. Zhang, P. Zheng, M. Zhao, J. Li, et al., High piezoelectric properties and domain configuration in  $\text{BaTiO}_3$  ceramics obtained through solid-state reaction route, *J. Phys. D: Appl. Phys.* 42 (2009) 189801.
- [22] W. Cai, Y. Fan, J. Gao, C. Fu, X. Deng, Microstructure, dielectric properties and diffuse phase transition of barium stannate titanate ceramics, *J. Mater. Sci. Mater. Electron.* 22 (2010) 265–272.
- [23] J.L. Chabel H., F.L. Zabotto, I.C. Nogueira, P. Schio, D. Garcia, O.F. de Lima, et al.,

- Magnetoelectric properties of laminated  $\text{La}_{0.7}\text{Ba}_{0.3}\text{MnO}_3\text{-BaTiO}_3$  ceramic composites, *J. Magn. Magn. Mater.* 364 (2014) 18–23.
- [24] R.B. von, D.C.A. Larson, The Regents of the University of California, Los Alamos National Laboratory, Los Alamos, USA, 2001.
- [25] G.V. Duong, R. Groessinger, M. Schoenhart, D. Bueno-Basques, The lock-in technique for studying magnetoelectric effect, *J. Magn. Magn. Mater.* 316 (2007) 390–393.
- [26] R.H. Buttner, E.N. Maslen, Structural parameters and electron difference density in  $\text{BaTiO}_3$ , *Acta Crystallogr. Sect. B Struct. Sci.* 48 (1992) 764–769.
- [27] E.M. Zoubaida El-Fadli, M. Redouane Metni, Fernando Sapiña, A.B. José-Vicente Folgado, Electronic properties of mixed-valence manganates: the role of Mn substitutional defects, *Chem. Mater.* 14 (2002) 688–696.
- [28] T. Sundararajan, S.B. Prabu, S.M. Vidyavathy, Combined effects of milling and calcination methods on the characteristics of nanocrystalline barium titanate, *Mater. Res. Bull.* 47 (2012) 1448–1454.
- [29] J. Zhou, H. He, Z. Shi, G. Liu, C.-W. Nan, Dielectric, magnetic, and magnetoelectric properties of laminated  $\text{PbZr}_{0.52}\text{Ti}_{0.48}\text{O}_3/\text{CoFe}_2\text{O}_4$  composite ceramics, *J. Appl. Phys.* 100 (2006) 094106.
- [30] H. Schmalzried, *Solid State Reactions*, Ed. 2, 1981.
- [31] R.L. Coble, Sintering crystalline solids. I. intermediate and final state diffusion models, *J. Appl. Phys.* 32 (1961) 787–792.
- [32] R.C. Rice, R.W. Pohanka, Grain-size dependence of spontaneous cracking in ceramics, *J. Am. Ceram. Soc.* 61 (1979) 559–563.
- [33] M.H. Frey, Z. Xu, P. Han, D.A. Payne, The role of interfaces on an apparent grain size effect on the dielectric properties for ferroelectric barium titanate ceramics, *Ferroelectrics* 206–207 (1998) 337–353.
- [34] O.P. Thakur, a Feteira, B. Kundys, D.C. Sinclair, Influence of attrition milling on the electrical properties of undoped- $\text{BaTiO}_3$ , *J. Eur. Ceram. Soc.* 27 (2007) 2577–2589.
- [35] Z. Zhao, V. Buscaglia, M. Viviani, M. Buscaglia, L. Mitoseriu, A. Testino, et al., Grain-size effects on the ferroelectric behavior of dense nanocrystalline  $\text{BaTiO}_3$  ceramics, *Phys. Rev. B* 70 (2004) 024107.
- [36] A.K. Jonscher, *IEEE Electr. Insul. Mag.* 6 (1990) 24–28, Part II.
- [37] L. Ca, M. Phan, S. Tian, S. Yu, A.N. Ulyanov, Magnetic and magnetocaloric properties of  $\text{La}_{0.7}\text{Ca}_{0.3-x}\text{Ba}_x\text{MnO}_3$  compounds, *J. Magn. Magn. Mater.* 256 (2003) 306–310.
- [38] K.R., C.N.R.R. Asish K Kundu, Md.Motin Seikh, Novel effects of size disorder on the electronic and magnetic properties  $\text{La}_{0.7}\text{Ba}_{0.3}\text{MnO}_3$ , *J. Phys. Condens. Matter* 17 (2005) 4171–4180.
- [39] R. Pazik, D. Kaczorowski, D. Hreniak, W. Strek, W. Łojkowski, Synthesis, structure and magnetic properties of  $\text{BaTiO}_3$  nanoceramics, *Chem. Phys. Lett.* 452 (2008) 144–147.
- [40] P. Kameli, H. Salamati, a Aezami, Influence of grain size on magnetic and transport properties of polycrystalline  $\text{La}_{0.8}\text{Sr}_{0.2}\text{MnO}_3$  manganites, *J. Alloy. Compd.* 450 (2008) 7–11.
- [41] F. Millange, V. Caignaert, B. Domenge, B. Raveau, Order-disorder phenomena in new  $\text{LaBaMn}_2\text{O}_{6-x}$  CMR perovskites. Crystal and magnetic structure, *Chem. Mater.* 4756 (1998) 1974–1983.
- [42] N. Zhang, W. Ding, W. Zhong, D. Xing, Y. Du, Tunnel-type giant magnetoresistance in the granular perovskite  $\text{La}_{0.85}\text{Sr}_{0.15}\text{MnO}_3$ , *Phys. Rev. B* 56 (1997) 8138–8142.
- [43] M. a Lopez-Quintela, L.E. Hueso, J. Rivas, F. Rivadulla, Intergranular magnetoresistance in nanomanganites, *Nanotechnology* 14 (2003) 212–219.
- [44] S.V. Trukhanov, a V. Trukhanov, S.G. Stepin, H. Szymczak, C.E. Botez, Effect of the size factor on the magnetic properties of manganite  $\text{La}_{0.50}\text{Ba}_{0.50}\text{MnO}_3$ , *Phys. Solid State* 50 (2008) 886–893.